Food Chemistry: X 14 (2022) 100335

Contents lists available at ScienceDirect

Food Chemistry: X

journal homepage: www.sciencedirect.com/journal/food-chemistry-x

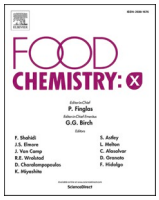

A potential spoilage bacteria inactivation approach on frozen fish

Linyu Nian [a,1], Mengjun Wang [a,1], Min Pan [a], Shujie Cheng [a], Wen Zhang [b], Chongjiang Cao [a,*]

[a] Department of Food Quality and Safety/National R&D Center for Chinese Herbal Medicine Processing, College of Engineering, China Pharmaceutical University, Nanjing 211198, China
[b] Crystal Infinity Environmental Technology Co., Ltd, Suzhou 215000, China

ARTICLE INFO

Keywords:
Spoilage bacteria
Inactivation
Ultrasound
High voltage electric field
Frozen food

ABSTRACT

Frozen products are more susceptible to microbial spoilage during thawing. Therefore, the development of a thawing technology with effective bacteriostasis is still urgent in food science. In this study, red sea bream was used as the research object, *S. putrefaciens* was incubated on the surface of fish fillets, and ultrasound plus high voltage electric field (US&HVEF) was performed to investigate the antibacterial activity. On this basis, the effect of US&HVEF thawing on the quality characteristics of fillets was further studied. The results indicated that US&HVEF showed a better antibacterial performance toward *S. putrefaciens*, with the lethality of 96.73%. Furthermore, US&HVEF could minimize thawing loss, preserve fillets texture, stabilize the secondary and tertiary conformation of myofibrillar protein (MFP), and inhibit the MFP aggregation and oxidation. Accordingly, this study shows that food safety also involves spoilage bacteria prevention except for quality and proves that US&HVEF technology has great potential in food thawing.

1. Introduction

Freezing storage plays a vital and widely effective preservation method for retaining the initial nutritional properties and sensory characteristics, and prolonging the shelf life of aquatic foodstuffs (Kong, Hamid, Liu, & Sarojini, 2016). As the reverse process of freezing, thawing is essential, however, aquatic products are more susceptible to microbial contamination and spoilage during the thawing process (Qiu, Zhang, Chitrakar, & Bhandari, 2020). It is estimated that 30 % of seafood is lost through microbial activity (Jääskeläinen et al., 2019). The predominant spoilage bacteria attached to refrigerated seafood are gram-negative bacteria, mainly *Pseudomonas* spp., *Aeromonas* spp., and *Shewanella* spp. (Sterniša, Klančnik, & Možina, 2019). In general, frozen fish was mainly suffered from *Shewanella* spp. during spoiling (Alfaro, Hernández, Marc, & Pin, 2013). Accordingly, it is urgent to seek efficient antibacterial technologies in the field of thawing aquatic products.

Ultrasonic thawing technology has attracted much more attention due to its highly efficient, nontoxic, and antimicrobial activity (Bhargava, Mor, Kumar, & Sharanagat, 2021; Qiu et al., 2020; Wu, Zhang, Adhikari, & Sun, 2017). Previous studies indicated that the antibacterial mechanisms of ultrasonication mainly include physical and chemical effects (Dai, Bai, Li, Cui, & Lin, 2020). Specifically, physical effects involve damage to the bacterial membrane by strong shearing forces, shock waves, micro jets, and turbulence, while chemical effects involve the generation of OH radicals and hydrogen peroxide induced by acoustic cavitation. However, the local temperature of the food surface was too high during ultrasonic thawing, resulting in deteriorating quality (Cai, Cao, Regenstein, & Cao, 2019). Therefore, individual ultrasound technology cannot achieve prospective effects in the quality maintenance of foodstuffs (Dai et al., 2020; Chen, Zhang, & Yang, 2019). Therefore, it is necessary to find a thawing technology to cooperate with ultrasonication to achieve an antimicrobial effect and quality maintenance, which has become a major research direction in the field of thawing.

As a uniform thawing technology, high voltage electric field (HVEF) has become one of the most promising technologies in food sterilization and preservation due to its maintenance of the original color, aroma and taste of food, and has no destructive effects on nutritional components (Amiri et al., 2019; Wyk, Silva, & Farid, 2019). In recent years, HVEF technology has been preliminarily applied to thawing aquatic products, such as common carp (Li et al., 2017a, Li et al., 2017b) and tuna fish (Mousakhani-Ganjeh, Hamdami, & Soltanizadeh, 2015, 2016a, 2016b). This showed that the technology has great potential in the thawing of aquatic products. In addition, due to its non-thermal properties, it can

* Corresponding author.
E-mail address: ccj33@163.com (C. Cao).
[1] These authors contribute equally in this work.

https://doi.org/10.1016/j.fochx.2022.100335
Received 30 August 2021; Received in revised form 19 April 2022; Accepted 15 May 2022
Available online 18 May 2022

compensate for the technical defects of ultrasonic thawing. In theory, US plus HVEF (US&HVEF) could supply a gap for a single technology to improve the quality maintenance of thawed foodstuffs.

Accordingly, *S. putrefaciens*, as the dominant representative spoilage bacteria of aquatic products, was collected in this study and incubated on red sea bream to investigate the spoilage microbe inactivation effect of US&HVEF. On this basis, the effect of US&HVEF thawing on the quality attributes of red sea bream was further constrained.

2. Materials and methods

2.1. Materials

Shewanella putrefaciens (i.e., *S. putrefaciens*, ATCC BAA-1097), as the dominant spoilage bacteria on aquatic products, was supplied by Beijing Biological Conservation Center to investigate the inactivation effect of bacteria using US&HVEF. Details of other chemical reagents are given in Section 1.1 of the Supplementary materials.

2.2. Sample preparation

The fillet samples were divided randomly into six groups: one positive control group, and five inoculated groups. For the positive control group, sterile fish fillets were immersed in sterile normal saline, which was called CON. For the inoculated groups, the sterile fish fillets were immersed in inoculation bacteria suspension. Then the inoculated groups were divided randomly into five groups, four of which were stored at −20 °C for 48 h, and thawed at room temperature (RT), high voltage electric field (HVEF), ultrasound (US), and US plus HVEF (US&HVEF). The fish fillets that were inoculated with *S. putrefaciens* and were not freeze–thawed were used as negative controls and named Control.

2.2.1. Preparation of sterile fish fillets

Sterile fish fillets were prepared according to Macé et al. (2013), Liu et al. (2018), and Lou, Zhai, and Yang (2020). (Details are provided in 1.2.1 of Supplementary materials).

2.2.2. Strain cultivation and inoculation

The *S. putrefaciens* was cultured in LB liquid medium and shaken at 200 rpm for 48 h at 30 °C using a whole temperature vibrator (THZ-C-1, Peiying Experimental Equipment Co., ltd., Suzhou, China). Then, the bacterial solution was washed with sterile normal saline for three times. After that, the bacterial solution was further diluted with sterile normal saline, until the OD_{600} value was approximately 0.1 using a microplate reader (Multiskan GO, Thermo Fisher Scientific, Waltham, MA, USA), and the bacteria were approximately concentrated to 10^8 CFU mL^{-1}. The bacterial suspension was serially diluted (1:10, sterile normal saline) to obtain a microbiological number of 10^6 CFU mL^{-1}.

To investigate the inactivation effect of US&HVEF against *S. putrefaciens* on red sea bream surfaces, *S. putrefaciens* was inoculated on the surfaces of fish fillets, as detail description in Supplementary materials 1.2.2.

2.2.3. Fillets thawing

The thawing device of fillets is shown in Fig. 1. The specific steps of the fillets were thawed by RT, HVEF, US, and US&HVEF can be found in Supplementary materials 1.2.3.

2.3. Determination the inactivation effect

Every block of inoculated groups' fish fillets, including Control, RT, HVEF, US, and US&HVEF, was smashed and then oscillated for 10 min with 20 mL sterile normal saline, and the mixture was filtered by sterile gauze to remove the meat residue. The filtrate was harvested to conduct colony-counting, SEM, and bacterial DNA and total protein extraction experiments.

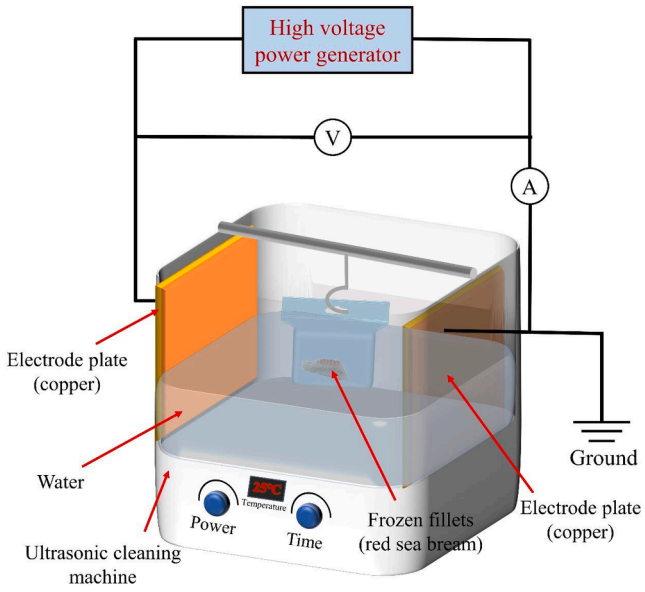

Fig. 1. Schematic diagram of red sea bream fillet thawing.

2.3.1. Antibacterial activity test

S. putrefaciens was plated on LB solid medium and cultured at 30 °C for 48 h to count the colony forming unit (CFU) number. The number of colonies on the plate was calculated by ImageJ software. Antibacterial efficiency was calculated based on Han et al. (2020), as detail description in Supplementary materials 1.3.1.

2.3.2. Morphology of S. putrefaciens

To directly reflect the morphology of bacteria, scanning electron microscope (SEM) of *S. putrefaciens* was slightly modified from Han et al. (2020), as detail description in Supplementary materials 1.3.2.

2.3.3. DNA of S. putrefaciens

DNA was extracted with a TIANamp Bacteria DNA Kit (DP302-01). Then, agarose gel electrophoresis (AGE) was performed at 100 V in 1 × TAE buffer (Shi et al., 2020). The DNA concentration was further confirmed using an ultra-micro ultraviolet spectrophotometer (Thermo Scientific NanoDrop™ One/One c) at a wavelength of 260 nm (OD_{260}) (Yu et al., 2019).

2.3.4. Total protein of S. putrefaciens

Total protein was extracted using the instructions of the Bacterial Protein Extraction Kit (KGP450). Then, sodium dodecyl sulfate polyacrylamide gel electropheresis (SDS-PAGE) was performed at 60 V for the stacking gel and 120 V for the resolving gel (Shi et al., 2020). The detail procedure of AGE and SDS-PAGE was shown in Supplementary materials 1.3.3.

2.4. Determination of fish quality

Furthermore, the effects of thawing treatments (RT, HVEF, US, and US&HVEF) on the quality of inoculated group fish fillets were investigated, including fillet muscle quality traits and myofibrillar protein (MFP) characteristics. Sterile fish fillets were used as a positive control group (CON).

2.4.1. Quality traits of fillets muscle

Thawing loss, pH value, and texture of fillets muscle were measured to evaluate the physicochemical characteristics of fish quality, and the detail procedure could be found in the Supplementary materials 1.4.

2.4.2. MFP characteristics of fillets

2.4.2.1. MFP extraction. The extraction method of MFP from red sea bream was slightly modified from Nian, Cao, & Cai (2020). Details on MFP extraction are provided in Supplementary materials 1.5.

2.4.2.2. MFP oxidation and degradation. T-SH content, carbonyl content, and Ca^{2+}-ATPase activity of the protein were measured using a total sulfhydryl content kit (A063-1), carbonyl content kit (A087), and ATPase kit (A070-3), respectively. SDS-PAGE of MFP was produced based on Cai et al. (2018), as detail description in Supplementary materials 1.6.

2.4.2.3. MFP conformation. Raman, Intrinsic fluorescence, and ultraviolet second derivative spectra of MFP were performed to explore MFP secondary and tertiary structure changes, as detail description in Supplementary materials 1.7.

2.4.2.4. MFP aggregation. The zeta-potential and particle size of MFP were determined using a Litesizer™ 500 nanoparticle size analyzer

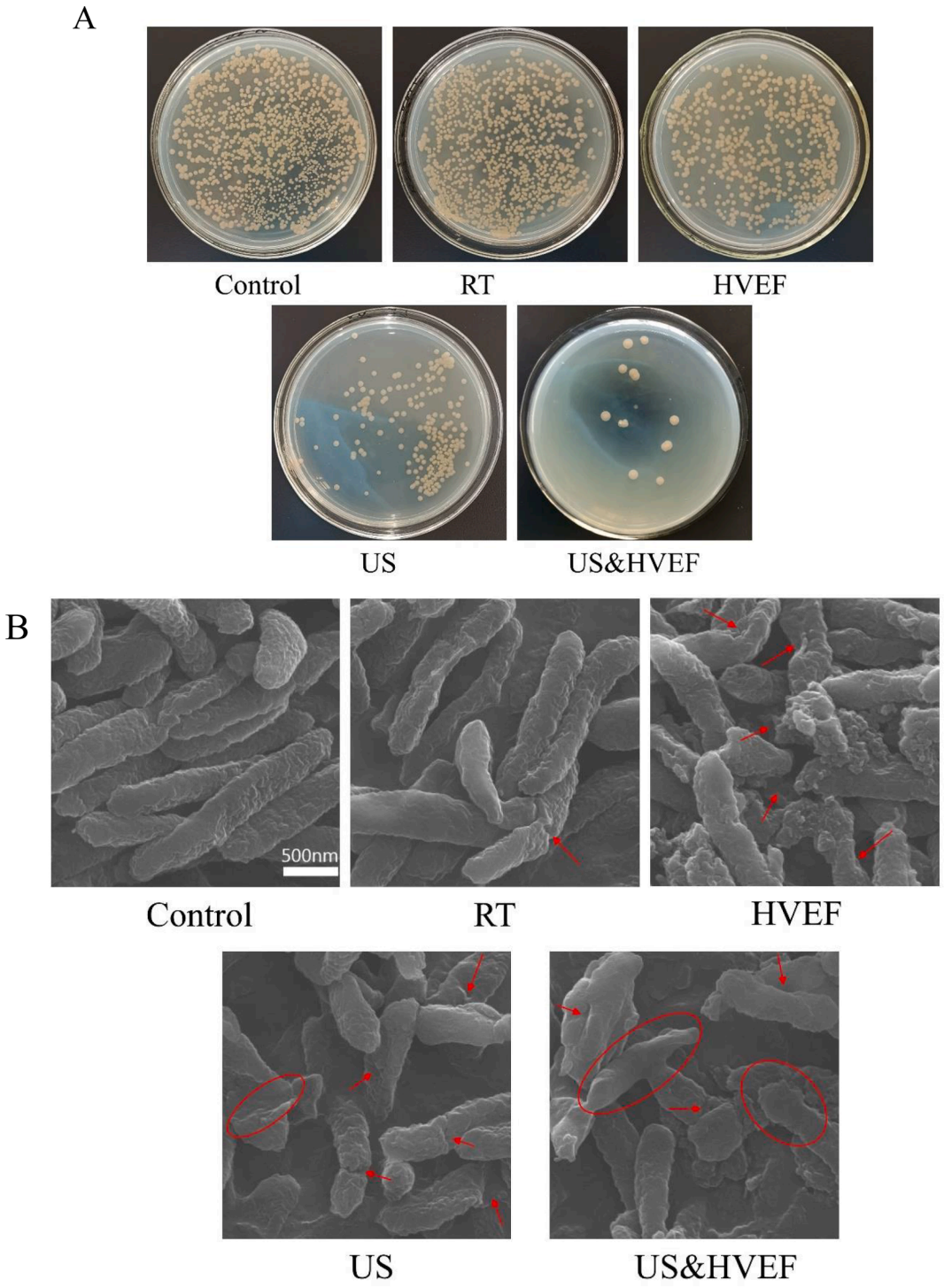

Fig. 2. The in vitro antibacterial activity of HVEF, US, US&HVEF treatment against *S. putrefaciens* (A); SEM images representing the morphologies and structures of *S. putrefaciens* (B); AGE assayed the concentration of DNA from *S. putrefaciens* (C); SDS-PAGE assayed the concentration of protein from *S. putrefaciens* (D).

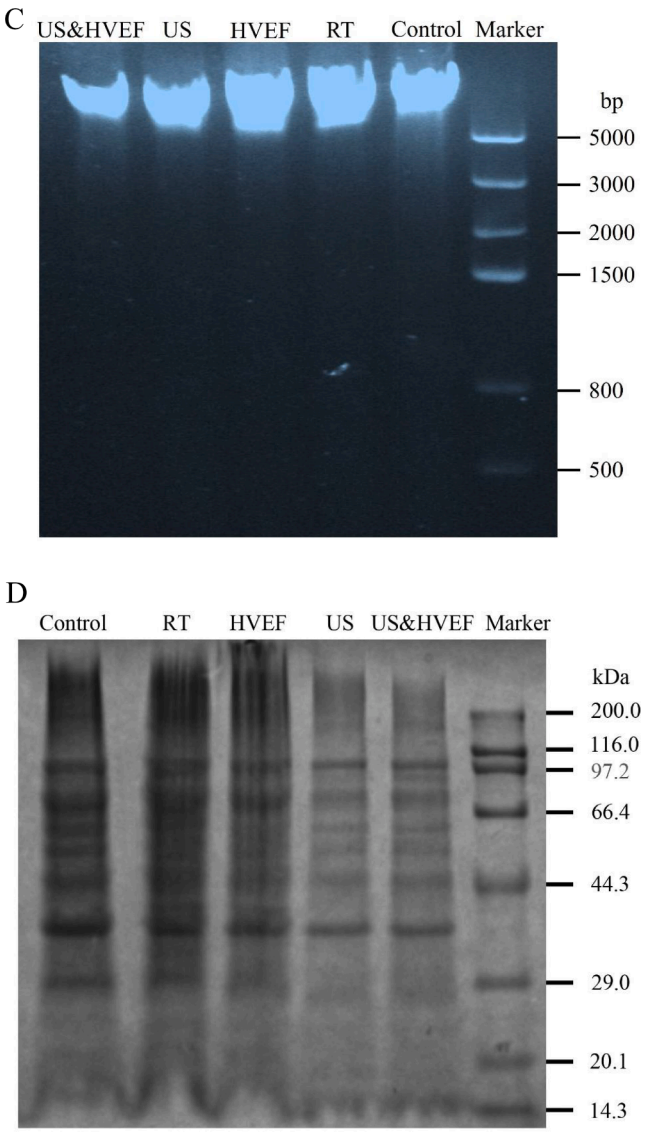

Fig. 2. (*continued*).

(Anton Paar Trading Co., ltd., Austria) equipped with a semiconductor laser/40 mW as the light source. The optical signal frequency was 658 nm, the detection method was dynamic light scattering, and the measuring angle was 90°.

2.5. Data analysis

All data are presented as the mean values and standard deviations, which were compared using one-way analysis of variance (ANOVA). Duncan's multiple range test was used to show the differences among mean values using SPSS 19 (SPSS Inc., Chicago, IL, USA). Specific parameters are as follows: One-way ANOVA: Post Multiple Comparisons, Polynomial; Degree: linear; Equal variances assumed: LSD and Duncan; Significance level: 0.05; Statistics: description. The number of colonies in the plate was calculated by ImageJ software (National Institutes of Health, USA). Raman spectra were analyzed by PeakFit Version 4.12 software (SPSS Inc). Figures were obtained by Origin Pro 8.5 (OriginLab Co., Northampton, MA, USA).

3. Results

3.1. Antibacterial efficiency

3.1.1. Occurrence of S. putrefaciens

As shown in Fig. 2A, visible colonies of *S. putrefaciens* thrived on LB agar plates after culture (Control). RT thawing has no obvious damage on *S. putrefaciens*. However, the bacterial colonies on fillets decreased by 47.12 %, 72.51 %, and 96.73 % after being thawed by HVEF, US, and US&HVEF, respectively (Fig. S1).

To characterize the morphology of *S. putrefaciens* after HVEF, US, and US&HVEF treatment, SEM results are provided in Fig. 2B. The bacteria were intact and plump-shaped in Control and RT samples with smooth and undeformed cell membranes. However, the *S. putrefaciens* treated with HVEF, US, and US&HVEF displayed a deformed and distorted shape with roughness, wrinkling, and damage accompanied by lesions and holes (Fig. 2B). In particular, the bacterial cells were absolutely ruptured and distorted after US&HVEF treatment (Fig. 2B).

In addition, the leakage of intracellular biomolecules (e.g., nucleic acids and proteins) was generally detected to investigate the inactivation path of *S. putrefaciens* by US&HVEF treatment, as shown in Fig. 2C.

3.1.2. DNA of S. putrefaciens

Compared with the Control, the fluorescence intensity of bacterial DNA, treated with RT, HVEF, and US did not exhibit a reduction. However, the fluorescence intensity of bacterial DNA extracted from US&HVEF samples decreased (Fig. 2C). Similarly, the DNA concentrations of the Control, RT, HVEF, US and US&HVEF samples were 144.4 ng/μL, 174.7 ng/μL, 231.5 ng/μL, 144.5 ng/μL, and 117.78 ng/μL, respectively (Fig. S2).

3.1.3. Total protein of S. putrefaciens

SDS-PAGE experiments to trace the leakage or damage of bacterial proteins were conducted to investigate the lethal effect of *S. putrefaciens* by US&HVEF. As displayed in Fig. 2D, compared with the Control, the intensity of the protein band in HVEF, US, and US&HVEF samples decreased, while RT samples showed no significant difference ($p \geq 0.05$). Similarly, the optical density values of bacterial total protein after HVEF, US, and US&HVEF treatment were significantly decreased to 223.16, 183.8, and 141.42, respectively, compared with the Control (316.24) and RT (291.04) (Fig. S3).

3.2. Fish quality

3.2.1. Quality traits of fillets muscle

As important indicators to evaluate quality, the thawing loss, pH, hardness, chewiness, and firmness of the fillet muscle after treatment with RT, HVEF, US, and US&HVEF were tested, as shown in Table 1. The values of pH are 7.36, 7.29, 7.25, and 7.21, and thawing loss are 8.87 %, 5.58 %, 6.08 %, and 4.07 %, and hardness are 108.13 g, 141.06 g, 190.18 g, and 255.81 g, and the chewiness are 286.97 g.sec, 365.48 g.sec, 476,73 g.sec, and 565.41 g.sec, and the firmness are −1.14 g.sec, −1.97 g.sec, −3.17 g.sec, and −3.38 g.sec for fillets after RT, HVEF, US, and US&HVEF treating, respectively. The pH values were positively correlated with thawing loss (the correlation coefficient (r) value = 0.935), while the hardness, chewiness, and firmness values were negatively correlated with thawing loss, with r values of −0.859, −0.865, and −0.833, respectively, as exampled by RT thawing fillets that have the highest pH values and thawing loss with a power texture (Table 1).

3.2.2. MFP characteristics of fillets

MFP accounts for 55 % ~ 60 % of muscle protein, and plays a decisive role in meat quality. Furthermore, the oxidation, degradation, aggregation and conformational changes of MFP after thawing were investigated to reflect the quality of fish. First, the oxidation degree of MFP was analyzed by the content of *T*-SH, carbonyl, and Ca^{2+}-ATPase activity, as shown in Fig. 3A.

3.2.2.1. MFP oxidation and degradation. Compared with CON (0.174 mmol/g *prot*), the *T*-SH contents of RT, HVEF, US, and US&HVEF were reduced by 0.071 mmol/g *prot*, 0.051 mmol/g *prot*, 0.048 mmol/g *prot* and 0.026 mmol/g *prot*, respectively. The carbonyl content increased to 1.957 nmol/mg *prot*, 1.64 nmol/mg *prot*, 1.483 nmol/mg *prot*, and 1.085 nmol/mg *prot*, respectively, compared with the CON sample (0.821 nmol/mg *prot*). The Ca^{2+}-ATPase activity decreased to 4.08 U/mg *prot*, 4.52 U/mg *prot*, 4.85 U/mg *prot*, and 5.34 U/mg *prot*, respectively, compared with the CON sample (5.91 U/mg *prot*).

SDS-PAGE experiments were then performed to investigate the degree of MFP degradation, as displayed in Fig. 3B. The electrophoretic bands were distributed at 15–200 kDa, mainly including myosin heavy chain (MHC, approximately 200 kDa), actinin (97.2 kDa), actin (42 kDa), troponin T (37 kDa), tropomyosin (36 kDa), and troponin I (18–21 kDa), and the results were similar to those of Cai et al. (2018). Furthermore, the electrophoretic bands were quantified by Quantity-One software, and the optical density distribution curve is shown in Fig. S4. Then, the sum of the optical density values of MHC and actin was calculated to characterize the degradation of MFP, as shown in Fig. 3C. Compared with CON samples (74), the density values of RT, HVEF, US, and US&HVEF decreased to 16.5, 38.4, 46.5, and 53.7, respectively. The density value of the RT samples was significantly lower than that of the other groups ($p < 0.05$), which was in accordance with Fig. 3C (MHC and actin showed shallow electrophoresis bands in the RT sample).

In addition, the spatial conformational (including secondary and tertiary structures) changes of MFP were investigated by Raman spectroscopy, intrinsic fluorescence spectroscopy, and UV second derivative spectroscopy.

3.2.2.2. MFP conformation. The stretching vibration intensity of phenylalanine at 1003 cm^{-1} was normalized as the internal standard, and the Raman spectrum of MFP was obtained from Fig. 4A, of which the amide I band (1600 ~ 1700 cm^{-1}) underwent deconvolution and curve fitting, as shown in Fig. S5. Then, the secondary structure of MFP, including α-helix (1645 ~ 1658 cm^{-1}), random coil (1660 ~ 1665 cm^{-1}), β-sheet (1665 ~ 1680 cm^{-1}), and β-turn (1680 cm^{-1}) (Cai et al., 2018; Zhang et al., 2020b), was quantified using Peakfit software. From Fig. 4B, the secondary structure of MFP from the CON sample was primarily α-helix, accounting for 58 %, while the random coil content was 9.27 %. Compared with CON, the fillets were thawed by RT, HVEF, US, and US&HVEF, the α-helix content decreased to 30.12 %, 35.87 %, 40.30 %, and 47.25 %, respectively, while the random coil content increased to 25.04 %, 22.89 %, 18.43 %, and 13.94 %, respectively.

The Raman spectrum at 500 ~ 550 cm^{-1} is the characteristic stretching vibration band of disulfide bridges (S—S). The conformations of S—S at 515–525 cm^{-1} and 535–545 cm^{-1} correspond to *gauche*-gauche-trans (g-g-t) and *trans*-gauche-trans (*t*-g-t), respectively, among which the *t*-g-t conformation is more stable (Herrero, 2008; Wang et al., 2020, Wang et al., 2020). From Fig. 4 C, compared with CON, US and US&HVEF (*t*-g-t), the conformation of disulfide bridges in RT and HVEF samples was transformed into g-g-t.

Furthermore, the intrinsic fluorescence spectrum can be used to reflect changes in the micro-environment of Trp residues, which is an important technical method to detect protein tertiary conformations. From Fig. 5A and 5B, the MFP of CON showed the highest fluorescence intensity (FI) (795.3) at the maximum position of the fluorescence peak (λ^{max}) (332.3 nm). Compared with CON, the λ^{max} of RT, HVEF, US, and US&HVEF showed a red shift (to longer wavelengths) of 2.1, 1.3, 1.0, and 0.5 nm, respectively. The FI decreased to 339.84, 433.67, 477.23, and 554.47 nm, respectively, and the FI value of US&HVEF was obviously higher than those of HVEF and US ($p < 0.05$).

The distance between the peak and trough of the first and second absorption peaks in the UV second derivative absorption spectrum was recorded as “a” and “b”, respectively (Fig. 5C). The r value (r = a/b) represents the change in polarity of the Tyr residue microenvironment and the protein structural unfolding (Cai et al., 2018). From Fig. 5C, the r values after HVEF, US, and US&HVEF treatment were significantly

Table 1
Thawing loss, pH and TPA (hardness, chewiness and firmness) of red sea bream treated by different thawing methods.[a,b]

Samples	Thawing loss (%)	pH	Hardness (g)	Chewiness (g.*sec*)	Firmness (g.*sec*)
CON	—	7.14 ± 0.01[d]	357.95 ± 15.92[a]	780.31 ± 9.95[a]	−6.66 ± 0.71[a]
RT	8.87 ± 1.32[a]	7.36 ± 0.03[a]	108.13 ± 5.23[e]	286.97 ± 35.32[e]	−1.14 ± 0.29[d]
HVEF	6.08 ± 0.87[b]	7.29 ± 0.01[b]	141.06 ± 7.78[d]	365.48 ± 36.70[d]	−1.97 ± 0.57[c]
US	5.58 ± 0.66[bc]	7.25 ± 0.02[c]	190.18 ± 5.63[c]	476.73 ± 68.07[c]	−3.17 ± 0.39[b]
US&HVEF	4.07 ± 1.03[c]	7.21 ± 0.02[c]	255.81 ± 17.44[b]	565.41 ± 12.97[b]	−3.38 ± 0.54[b]

[a] All values were means ± standard deviation of three values.
[b] Different lowercases in the same row indicate significant differences between means ($p < 0.05$).

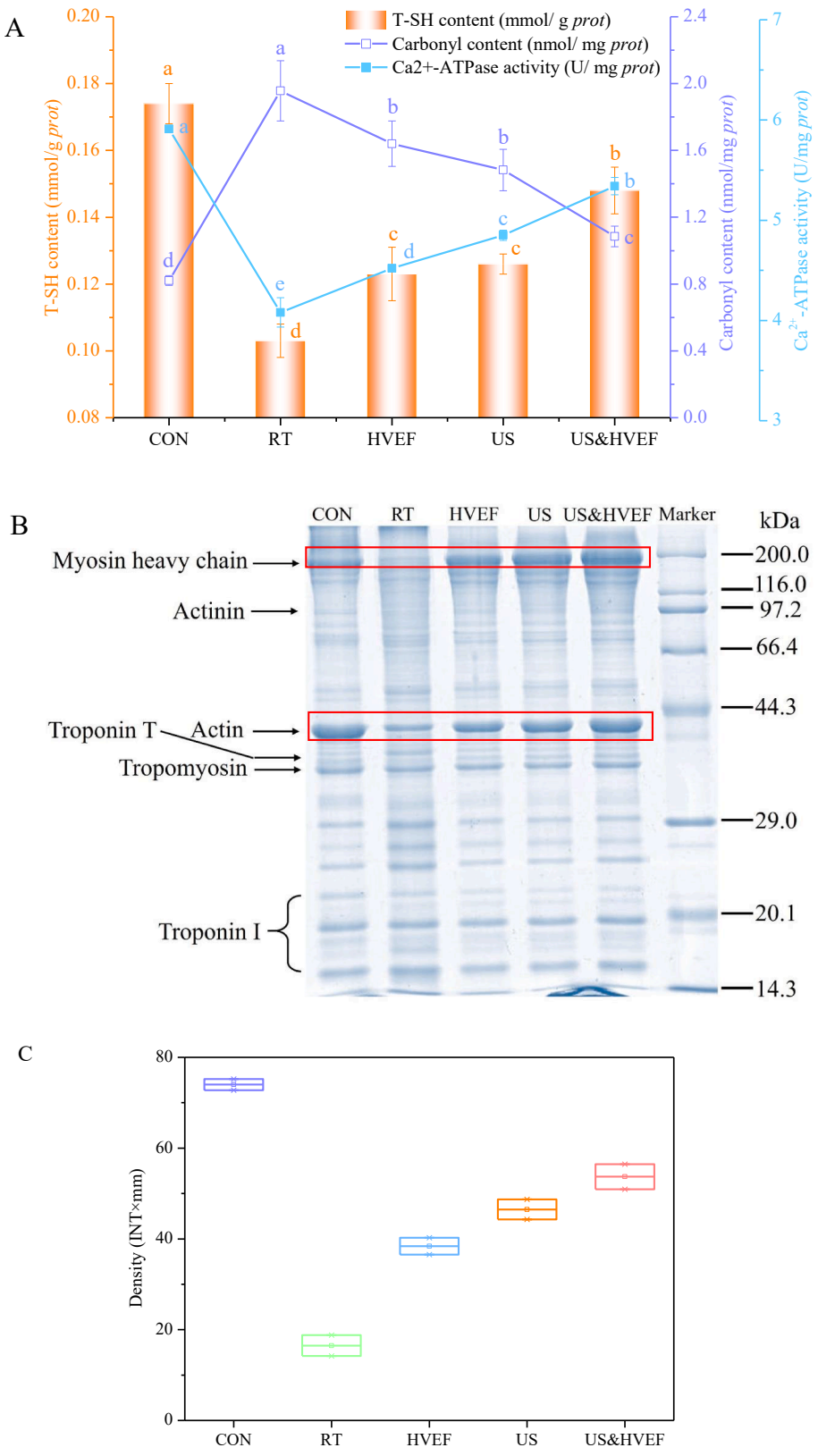

Fig. 3. Changes in the oxidation of myofibrillar protein (content of *T*-SH, carbonyl, and Ca2 + -ATPase activity) from red sea bream (A); SDS-PAGE of myofibrillar protein from red sea bream (B); Optical density values of myosin heavy chain (MHC) and actin (C). (Different lowercase letters in orange, purple and blue indicate significant differences between the means of *T*-SH content, carbonyl content and Ca^{2+}-ATPase activity, respectively in Fig. 3A ($p < 0.05$)).

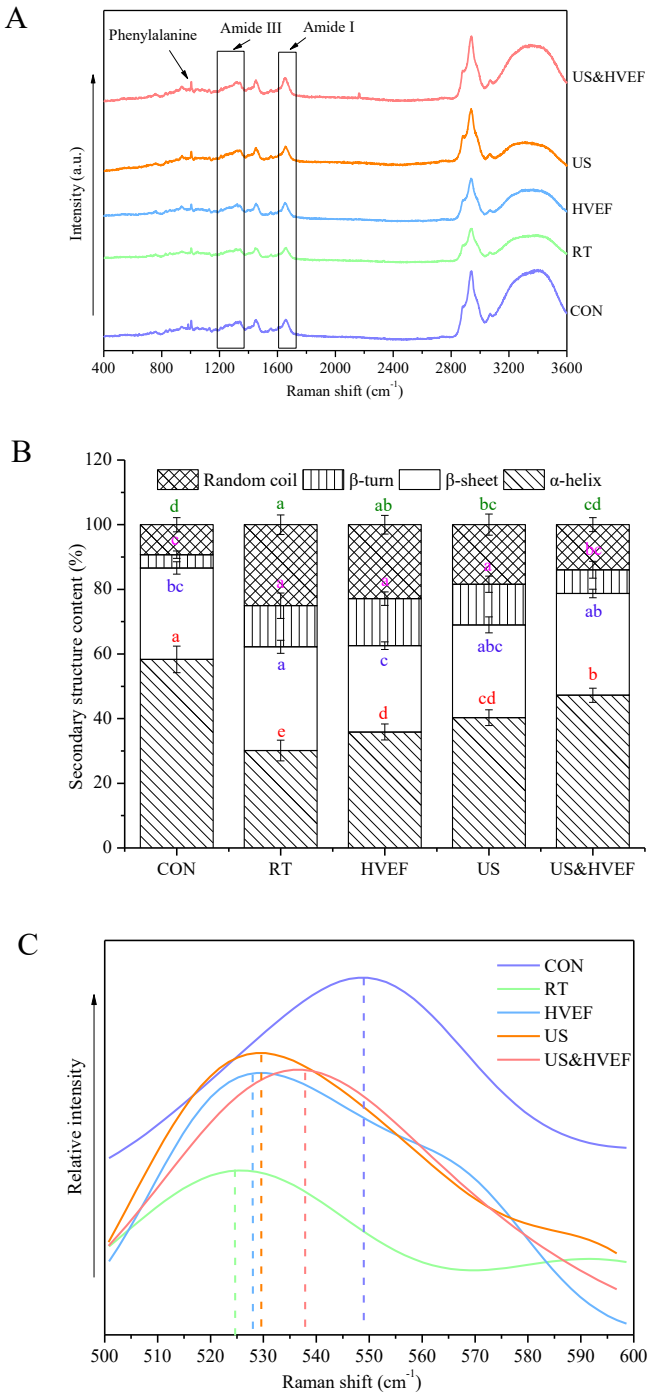

Fig. 4. Raman spectra (A); Secondary structure content (B); C: Disulfide bridges (C) of myofibrillar protein from red sea bream treated by different thawing methods. (Different lowercase letters in red, blue, pink and green indicate significant differences between the means of α-helix, β-sheet, β-turn and random coil content, respectively in Fig. 4B ($p < 0.05$)).

increased by 0.92 %, 9.17 %, and 3.67 %, respectively, compared with the RT sample (1.09).

Then, the aggregation degree of MFP was characterized by zeta-potential and particle size, as displayed in Fig. 5D and Fig. S6.

3.2.2.3. MFP aggregation. The ζ value of the MFP solution from the CON sample was −43.27 mV, implying the good stability of solution. After the fillets were thawed by RT, HVEF, US, and US&HVEF, the ζ values of MFP solution were –23.52 mV, −29.26 mV, –33.56 mV, and −36.82 mV, respectively (Fig. 5D). The average effective particle diameter (d_{eff}) was 2641.84 nm, 1920.89 nm, 1621.94 nm, and 1340.06 nm, respectively, as compared with CON (1037.18 nm) (Fig. 5D and Fig. S6).

4. Discussion

4.1. Analyses of antibacterial efficiency

S. putrefaciens was incubated on the surface of red sea bream fillets, and the antibacterial efficiency of HVEF, US, and US&HVEF technologies was investigated by SEM, AGE, and SDS-PAGE experiments. Results indicated that RT treatment had no damaging effect on *S. putrefaciens*. When *S. putrefaciens* was treated with HVEF, US and US&HVEF, the cell membrane was disrupted and broken. In particular, bacterial cells were absolutely ruptured and distorted after US&HVEF treatment (Fig. 2B).

Previous studies have proven that the inactivation of bacteria caused by HVEF was as follows: 1) The ozone produced by ionization of the air, leading to perforation polarization and rupture of the bacterial cell membrane. 2) The transmembrane voltage of the cell membrane increased gradually under the action of electric field, leading to the thinning of the cell membrane and the formation of micropores, furthermore, cell membrane ruptures when the threshold of trans-membrane voltage was exceeded, resulting in the loss of juice in the membrane (Mousakhani-Ganjeh et al., 2015, 2016; Qi et al., 2020). In addition, the bacterial inactivation mechanism by US is widely considered to be a combination of mechanical, thermal, and chemical effects when cavitation bubbles collapse (Chen et al., 2012; Dai et al., 2020). Specifically, mechanical effects are involved in damage to the bacterial membrane by strong shearing forces, shock waves, micro-jets, and turbulence. The thermal effects refer to the heat generated by cavitation bubbles increasing the temperature of the liquid around the bubbles and creating a local hot spot, which causes irreversible damage to cells. The chemical effects are involved in the generation of OH– radicals and hydrogen peroxide induced by acoustic cavitation. Accordingly, US&HVEF showed a synergistic bacteriostatic effect on the rupture of bacterial cell membranes.

To further demonstrated the killing mechanism of *S. putrefaciens* by the treatment of HVEF, US, and US&HVEF, the leakage of intracellular biomolecules, such as nucleic acid and protein was investigated. AEG was used to study the leakage or damage of bacterial DNA (Fig. 2C), and the DNA concentration was quantified by the optical value of the DNA solution at OD_{260} (Fig. S2). Results demonstrated that the DNA of *S. putrefaciens* could not be damaged or leaked under the treatment of individual US or HVEF, but the *S. putrefaciens* under the treatment of US&HVEF, the obtained DNA concentration were obviously decreased compared to the individual US or HVEF technology. Furthermore, SDS-PAGE was used to study the leakage or damage of bacterial protein (Fig. 2D), and electrophoresis bands were quantified using Quantity-One software. After Gauss modeling, the optical density of each strip could be calculated, and the total of optical density values of all bands were represented the total protein content, which displayed in Fig. S3. The density values of HVEF, US and US&HVEF were significantly decreased ($p < 0.05$) compared to control, especially in US&HVEF group, the obvious degradation of bacterial protein was observed, which indicated that the bacterial protein to leakage under the treatment of US&HVEF. Accordingly, we proposed the potential antimicrobial mechanism for US&HVEF: US&HVEF treatment destroyed the cell membrane and caused the intracellular biomolecules (e.g., nucleic acid and protein) to damage and leakage, resulting in the death of bacteria (i.e., *S. putrefaciens*).

4.2. Analyses of thawing quality of fish fillets

In view of the antibacterial effect of US&HVEF on *S. putrefaciens*, its effects on the quality characteristics of fillets were further discussed.

The linear relationship between antibacterial efficiency and fish

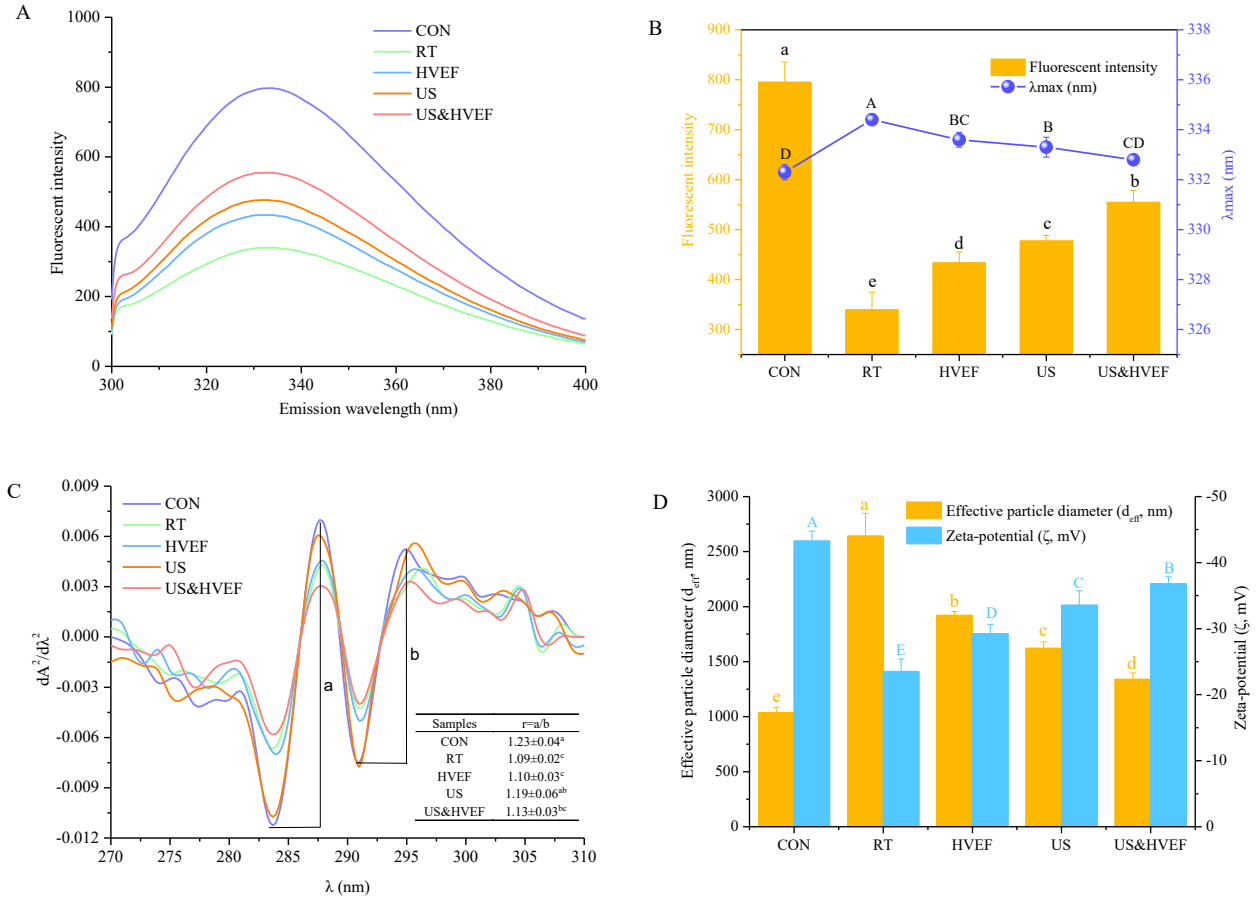

Fig. 5. Intrinsic fluorescence spectra (A); Fluorescent intensity and maximum position of fluorescence peak (λ^{max}) (B); UV second derivative spectra (C); Zeta-potential (ζ) and effective particle diameter (d_{eff}) of myofibrillar protein from red sea bream (D) treated by different thawing methods. (Different lowercase and uppercase letters indicate significant differences between the means of fluorescent intensity and λ^{max}, respectively in Fig. 5B ($p < 0.05$); Different lowercase and uppercase letters indicate significant differences between the means of d_{eff} and ζ, respectively in Fig. 5D ($p < 0.05$)).

meat quality was explored, and it was found that the antibacterial efficiency was negatively correlated with the thawing loss and pH value of fish meat, with r values of −0.925 and −0.999, respectively. The pH value can reflect the degree of muscle corruption. When aquatic products are softened and corruption, proteins and nitrogen-containing substances will be decomposed into amino acids, ammonia, trimethylamine, hydrogen sulfide, indole, and some other alkaline substances, resulting in the increases of pH (Liu et al., 2013). Based on the discussion of Section 4.1, US&HVEF treatment has a synergistic inhibitory effect on the growth of microorganisms, which could decrease the accumulation of alkaline products, control the change of pH, and maintain the fillets quality.

The hardness, chewiness, and firmness values were positively correlated with the antibacterial efficiency, and the r values were 0.967, 0.987, and 0.976, respectively. According to He et al. (2016), the fracture of hydrogen bonds among ice was accelerated by the action of an electric field, leading to ice existing in the form of small ice crystals, which reduced the damage of the ice crystals to the foodstuffs. In addition, turbulence was generated when ultrasonic waves disseminated through the thawed liquid, which improved the heat transmission efficiency and reduced food damage (Cai et al., 2019). Therefore, the fillets thawed by HVEF or US, displayed lower thawing loss and higher quality compared to RT samples. The quality maintenance of fillets thawed by US&HVEF was better than that of a single HVEF or US thawing technology, which manifested in lower thawing loss and better texture. This was mainly because US&HVEF could improve the inhibitory effect on the growth of microorganisms (antibacterial efficiency was 96.73 %).

Next, MFP was used as an entry point to explore the quality characteristics of fish, and mainly the oxidation, degradation, aggregation and conformational changes of MFP were studied.

Previous studies have proven that a series of complex reactions occur due to the oxidation of proteins, mainly manifesting in the following three aspects (Zhang et al., 2015; Davies, 2016; Nian et al., 2020): ① the loss of protein sulfhydryl groups; ② the formation of protein carbonyl groups; and ③ the production of protein cross-linking. Specifically, the T-SH content of protein plays an important role in stabilizing the spatial structure of protein and can be used to reflect the degree of protein oxidation (Nian et al., 2020). In addition, amino or imino groups in the side chains of amino acid residues were attacked by oxygen free radicals and converted into carbonyl groups, therefore, the formation of protein carbonyl was considered as a typical characteristic of protein oxidation, and the carbonyl content was used as an important indicator for determining the oxidation protein (Zhang et al., 2015). In addition, Ca^{2+}-ATPase activity represents the integrity of the structure of the myosin head, and the decrease in activity is due to the oxidation of sulfhydryl on the head of myosin (Zhang et al., 2020b). Therefore, the decrease in Ca^{2+}-ATPase activity was also a specific biomarker for protein oxidation. The degree of protein oxidation of fillets under different thawing methods by analyzing the *T*-SH/carbonyl content, Ca^{2+}-ATPase activity and SDS-PAGE in this article. From Fig. 3A, the US&HVEF sample displayed the highest *T*-SH content and Ca^{2+}-ATPase activity, and the lowest carbonyl content, compared with the RT, HVEF, and US samples. By analyzing the linear relationship between antibacterial efficiency and the degree of protein oxidation, the antibacterial efficiency was positively correlated with the *T*-SH content and Ca^{2+}-ATPase activity, and the r value was 0.968 and 0.991, respectively, while negatively

correlated with the carbonyl content, the r value was −0.980. Given the efficient bacteriostatic effect of US&HVEF technology as mentioned above, the fillet protein oxidation degree was significantly reduced (Fig. 3A).

The degradation of MFP can be analyzed by SDS-PAGE. The separation of proteins can be achieved through the molecular weight and charged properties of protein subunits (Zhang et al., 2020a), and the separated protein bands were further analyzed (Fig. 3B, 3C). The sum of the optical density values of MHC and actin were calculated in this paper to characterize the degradation of the MFP. The r value between antibacterial efficiency and the sum of the optical density values of MHC and actin was 0.985. From Fig. 3B, the MHC and actin showed shallow electrophoresis bands in RT sample, especially the MHC band almost disappeared, indicating that the oxidation and denaturation of MFP occurred when the frozen fillets were thawed at room temperature. Moreover, the density value of HVEF and US samples was significantly lower than that of the US&HVEF samples ($p < 0.05$). These confirmed US&HVEF samples have the weakest protein degradation degree, which attributed to the highest antibacterial efficiency of US&HVEF treatment.

Then, the fish quality was determined from the perspective of protein conformational changes. Raman spectroscopy was used to obtain the protein secondary structure, including α-helix, random coil, β-sheet, and β-turn, which is important for exploring the relationship between the protein secondary structure and the quality of samples (Herrero, 2008). α-helix and β-sheet represent the conformational regularity of proteins, while random coil and β-turn represent the conformational looseness of proteins (Nian et al., 2019). The r values between the antibacterial efficiency and α-helix, and random coil contents were 0.988, and −0.965, respectively. From Fig. 4B, the secondary structure of MFP from fresh fish (CON) was primarily α-helix, accounting for 58 %. The α-helix structure was maintained mainly by the hydrogen bond between the carbonyl oxygen (–CO) and the imino hydrogen (–NH-) of the polypeptide chain. After fillets were thawed, the α-helix content was decreased, while the random coil content was increased, which was attributed to the growth and reproduction of microorganisms on the fillets, and the damage of ice crystals to the fiber cells caused the oxidation and denaturation of fillets protein, resulting in the expansion of α-helix, and the damage of protein secondary structure (Wang et al., 2020, Wang et al., 2020). From Fig. 4B, After the fillets were thawed, US&HVEF samples showed the highest α-helix and the lowest random coils, which was due to the synergistic antibacterial effect and the poorer damage of ice crystals to fiber cells reduced the degree of protein oxidation and stabilize the secondary structure of protein.

In addition, the conformational changes of MFP can be effectively monitored by measuring the intrinsic fluorescence spectrum of Trp residues (Fig. 5B). In addition, UV second derivative absorption spectra were used to analyze the changes in the microenvironment of aromatic amino acid residues, such as tyrosine (Tyr) and tryptophan (Trp) (Fig. 5C). The results indicated that US&HVEF technology has a synergistic bacteriostatic effect, the degree of protein oxidation during thawing was reduced, which effectively maintained the stability of the protein spatial conformation.

Finally, the effect of US&HVEF thawing on the degree of protein aggregation was studied. Zeta-potential (ζ) was used to describe the electrostatic interactions between protein molecules. The higher the absolute value of the zeta-potential ($|\zeta|$), the stronger the electrostatic interaction between the protein particles, which could increase the electrostatic repulsion, and prevent protein molecules from aggregating, resulting in a smaller average effective particle diameter (d_{eff}) of the protein (Huang et al. 2019). Specifically, the ζ value ranged from −16 to −30 mV, which meant the threshold of delicate dispersion of protein solution, and from −30 to −40 mV indicated the moderate stability of solution (Beliciu & Moraru, 2011). From Fig. 5D, after fillets were thawed, the $|\zeta|$ value of US&HVEF samples was the highest, and the d_{eff} was the lowest, indicating that the electrostatic repulsion between protein molecules was enhanced, and the degree of aggregation in protein molecules was weakened, resulting in a smaller protein particle size and the enhanced solution stability. The linear relationship between antibacterial efficiency and the degree of protein aggregation was investigated. The antibacterial efficiency was positively correlated with $|\zeta|$, but negatively correlated with the average effective particle diameter (d_{eff}). The r value was 0.991 and −0.999, respectively.

5. Conclusion

This study revealed that US&HVEF has a high bacteriostatic effect on *S. putrefaciens*, and the antibacterial efficiency reached 96.73 %. Moreover, the antibacterial mechanism of US&HVEF toward *S. putrefaciens* was attributed to the disruption of the cell membrane, leakage and damage to DNA and protein. Furthermore, the thawing quality of fillets was markedly improved in US&HVEF and in comparison with the individual thawing technology, the specific performance of maintaining the stability of MFP tertiary conformation more effectively, and inhibiting the oxidation and aggregation of MFP. In summary, US&HVEF was efficient in maintaining the quality of fish during thawing, which could be attributed to its excellent microbial inactivation efficiency and the complementary advantages of HVEF and US technology.

CRediT authorship contribution statement

Linyu Nian: Conceptualization, Methodology, Software, Validation, Writing – original draft, Writing – review & editing. **Mengjun Wang:** Conceptualization, Methodology, Software, Validation, Writing – review & editing. **Min Pan:** Software, Writing – review & editing. **Shujie Cheng:** Writing – review & editing. **Wen Zhang:** Methodology. **Chongjiang Cao:** Writing – review & editing, Supervision.

Declaration of Competing Interest

The authors declare that they have no known competing financial interests or personal relationships that could have appeared to influence the work reported in this paper.

Acknowledgments

This study was supported by the National Key Research and Development Program of China (2019YFC1605800), the National Natural Science Foundation of China (32172272), Modern Agricultural Machinery Equipment and Technology Demonstration and Promotion Project of Jiangsu Province (NJ2021-20), and Jiangsu Agriculture Science and Technology Innovation Fund (CX(21)3171).

Appendix A. Supplementary data

Supplementary data to this article can be found online at https://doi.org/10.1016/j.fochx.2022.100335.

References

Alfaro, B., Hernández, I., Marc, Y. L., & Pin, C. (2013). Modelling the effect of the temperature and carbon dioxide on the growth of spoilage bacteria in packed fish products. *Food Control, 29*(2), 429–437.

Amiri, A., Mousakhani-Ganjeh, A., Shafiekhani, S., Mandal, R., Singh, A. P., & Kenari, R. E. (2019). Effect of high voltage electrostatic field thawing on the functional and physicochemical properties of myofibrillar proteins. *Innovative Food Science & Emerging Technologies, 56*, 102191. https://doi.org/10.1016/j.ifset.2019.102191

Beliciu, C. M., & Moraru, C. I. (2011). The effect of protein concentration and heat treatment temperature on micellar casein-soy protein mixtures. *Food Hydrocolloids, 25*(6), 1448–1460.

Bhargava, N., Mor, R. S., Kumar, K., & Sharanagat, V. S. (2021). Advances in application of ultrasound in food processing: A review. *Ultrasonics Sonochemistry, 70*, 105293. https://doi.org/10.1016/j.ultsonch.2020.105293

Cai, L., Cao, M., Cao, A., Regenstein, J., Li, J., & Guan, R. (2018). Ultrasound or microwave vacuum thawing of red seabream (*Pagrus major*) fillets. *Ultrasonics Sonochemistry, 47*, 122–132.

Cai, L., Cao, M., Regenstein, J., & Cao, A. (2019). Recent advances in food thawing technologies. *Comprehensive Reviews in Food Science and Food Safety, 18*(4), 953–970.
Cai, L., Zhang, W., Cao, A., Cao, M., & Li, J. (2019). Effects of ultrasonics combined with far infrared or microwave thawing on protein denaturation and moisture migration of Sciaenops ocellatus (*Red drum*). *Ultrasonics Sonochemistry, 55*, 96–104.
Chen, F., Zhang, M., & Yang, C. H. (2019). Application of ultrasound technology in processing of ready-to-eat fresh food: A review. *Ultrasonics Sonochemistry, 63*, Article 104953.
Chen, J. H., Ren, Y., Seow, J., Liu, T., Bang, W. S., & Yuk, H. G. (2012). Intervention technologies for ensuring microbiological safety of meat: Current and future trends. *Comprehensive Reviews in Food Science and Food Safety, 11*(2), 119–132.
Dai, J., Bai, M., Li, C., Cui, H., & Lin, L. (2020). Advances in the mechanism of different antibacterial strategies based on ultrasound technique for controlling bacterial contamination in food industry. *Trends in Food Science & Technology, 105*, 211–222.
Davies, M. J. (2016). Protein oxidation and peroxidation. *Biochemical Journal, 473*(7), 805–825.
Han, D., Han, Y., Li, J., Liu, X., Yeung, K. W. K., Zheng, Y., … Wu, S. (2020). Enhanced photocatalytic activity and photothermal effects of cu-doped metal-organic frameworks for rapid treatment of bacteria-infected wounds. *Applied Catalysis B: Environmental, 261*, Article 118248.
He, X., Jia, G., Tatsumi, E., & Liu, H. (2016). Effect of corona wind, current, electric field and energy consumption on the reduction of the thawing time during the high-voltage electrostatic-field (HVEF) treatment process. *Innovative Food Science & Emerging Technologies, 34*, 135–140.
Herrero, A. M. (2008). Raman spectroscopy for monitoring protein structure in muscle food systems. *Critical Reviews in Food Science and Nutrition, 48*(6), 512–523.
Huang, L., Ding, X., Li, Y., & Ma, H. (2019). The aggregation, structures and emulsifying properties of soybean protein isolate induced by ultrasound and acid. *Food Chemistry, 279*, 114–119.
Jääskeläinen, E., Jakobsen, L. M. A., Hultman, J., Eggers, N., Bertram, H. C., & Björkroth, J. (2019). Metabolomics and bacterial diversity of packaged yellowfin tuna (*Thunnus albacares*) and salmon (*Salmo salar*) show fish species-specific spoilage development during chilled storage. *International Journal of Food Microbiology, 293*, 44–52.
Kong, C. H. Z., Hamid, N., Liu, T., & Sarojini, V. (2016). Effect of antifreeze peptide pretreatment on ice crystal size, drip loss, texture, and volatile compounds of frozen carrots. *Journal of Agricultural and Food Chemistry, 64*(21), 4327–4335.
Li, D., Jia, S., Zhang, L., Li, Q., Pan, J., Zhu, B., … Luo, Y. (2017). Post-thawing quality changes of common carp (*Cyprinus carpio*) cubes treated by high voltage electrostatic field (HVEF) during chilled storage. *Innovative Food Science & Emerging Technologies, 42*, 25–32.
Li, D., Jia, S., Zhang, L., Wang, Z., Pan, J., Zhu, B., & Luo, Y. (2017). Effect of using a high voltage electrostatic field on microbial communities, degradation of adenosine triphosphate, and water loss when thawing lightly-salted, frozen common carp (*Cyprinus carpio*). *Journal of Food Engineering, 212*, 226–233.
Liu, D., Liang, L.i., Xia, W., Regenstein, J. M., & Zhou, P. (2013). Biochemical and physical changes of grass carp (*Ctenopharyngodon idella*) fillets stored at -3 and 0°C. *Food chemistry, 140*(1-2), 105–114.
Liu, X., Huang, Z., Jia, S., Zhang, J., Li, K., & Luo, Y. (2018). The roles of bacteria in the biochemical changes of chill-stored bighead carp (*Aristichthys nobilis*): Proteins degradation, biogenic amines accumulation, volatiles production, and nucleotides catabolism. *Food Chemistry, 255*, 174–181.
Lou, X. W., Zhai, D. D., & Yang, H. S. (2020). Changes of metabolite profiles of fish models inoculated with *Shewanella baltica* during spoilage. *Food Control, 107697*.
Macé, S., Joffraud, J.-J., Cardinal, M., Malcheva, M., Cornet, J., Lalanne, V., … Dousset, X. (2013). Evaluation of the spoilage potential of bacteria isolated from spoiled raw salmon (*Salmo salar*) fillets stored under modified atmosphere packaging. *International Journal of Food Microbiology, 160*(3), 227–238.
Mousakhani-Ganjeh, A., Hamdami, N., & Soltanizadeh, N. (2015). Impact of high voltage electric field thawing on the quality of frozen tuna fish (*Thunnus albacares*). *Journal of Food Engineering, 156*, 39–44.
Mousakhani-Ganjeh, A., Hamdami, N., & Soltanizadeh, N. (2016a). Effect of high voltage electrostatic field thawing on the lipid oxidation of frozen tuna fish (*Thunnus albacares*). *Innovative Food Science & Emerging Technologies, 36*, 42–47.
Mousakhani-Ganjeh, A., Hamdami, N., & Soltanizadeh, N. (2016b). Thawing of frozen tuna fish (*Thunnus albacares*) using still air method combined with a high voltage electrostatic field. *Journal of Food Engineering, 169*, 149–154.
Nian, L., Cao, A., & Cai, L. (2020). Investigation of the antifreeze mechanism and effect on quality characteristics of largemouth bass (*Micropterus salmoides*) during F-T cycles by hAFP. *Food Chemistry, 325*, 126918. https://doi.org/10.1016/j.foodchem.2020.126918
Nian, L., Cao, A., Cai, L., Ji, H., & Liu, S. (2019). Effect of vacuum impregnation of red sea bream (*Pagrosomus major*) with herring AFP combined with CS@Fe_3O_4 nanoparticles during freeze-thaw cycles. *Food Chemistry, 291*, 139–148.
Qi, M., Zhao, R., Liu, Q., Yan, H., Zhang, Y., Wang, S., & Yuan, Y. (2020). Antibacterial activity and mechanism of high voltage electrostatic field (HVEF) against *Staphylococcus aureus* in medium plates and food systems. *Food Control, 107566*.
Qiu, L., Zhang, M., Chitrakar, B., & Bhandari, B. (2020). Application of power ultrasound in freezing and thawing Processes: Effect on process efficiency and product quality. *Ultrasonics Sonochemistry, 68*, 105230. https://doi.org/10.1016/j.ultsonch.2020.105230
Shi, H., Fan, J., Zhao, Y., Hu, X., Zhang, X., & Tang, Z. (2020). Visible light driven $CuBi_2O_4/Bi_2MoO_6$ p-n heterojunction with enhanced photocatalytic inactivation of E. coli and mechanism insight. *Journal of Hazardous Materials, 381*, Article 121006.
Sterniša, M., Klančnik, A., & Smole Možina, S. (2019). Spoilage pseudomonas biofilm with escherichia coli protection in fish meat at 5 °C. *Journal of the Science of Food and Agriculture, 99*(10), 4635–4641.
Wang, B., Kong, B., Li, F., Liu, Q., Zhang, H., & Xia, X. (2020). Changes in the thermal stability and structure of protein from porcine longissimus dorsi induced by different thawing methods. *Food Chemistry, 316*, 126375. https://doi.org/10.1016/j.foodchem.2020.126375
Wang, B., Li, Y., Wang, H., Liu, X., Zhang, Y., & Zhang, H. (2020). In-situ analysis of the water distribution and protein structure of dough during ultrasonic-assisted freezing based on miniature Raman spectroscopy. *Ultrasonics Sonochemistry, 67*, 105149. https://doi.org/10.1016/j.ultsonch.2020.105149
Wu, X.-F., Zhang, M., Adhikari, B., & Sun, J. (2017). Recent developments in novel freezing and thawing technologies applied to foods. *Critical Reviews in Food Science and Nutrition, 57*(17), 3620–3631.
Wyk, S. V., Silva, F. V. M., & Farid, M. M. (2019). Pulsed electric field treatment of red wine: Inactivation of brettanomyces and potential hazard caused by metal ion dissolution. *Innovative Food Science & Emerging Technologies, 52*(2019), 57–65.
Yu, S., Li, G., Zhao, P., Cheng, Q., He, Q., Ma, D., & Xue, W. (2019). NIR-laser-controlled hydrogen-releasing PdH nanohydride for synergistic hydrogen-photothermal antibacterial and wound-healing therapies. *Advanced Functional Materials, 29*(50), 1905697. https://doi.org/10.1002/adfm.v29.5010.1002/adfm.201905697
Zhang, J., Zhou, D., Zhong, X., Pei, Z., Tian, Y., Xiang, D., … Li, C. (2020). Quality and protein degradation of golden pompano (*Trachinotus blochii*) fillets during four drying methods. *LWT, 130*, 109638. https://doi.org/10.1016/j.lwt.2020.109638
Zhang, L., Shan, Y., Hong, H., Luo, Y., Hong, X., & Ye, W. (2020). Prevention of protein and lipid oxidation in freeze-thawed bighead carp (*Hypophthalmichthys nobilis*) fillets using silver carp (*Hypophthalmichthys molitrix*) fin hydrolysates. *LWT, 123*, 109050. https://doi.org/10.1016/j.lwt.2020.109050
Zhang, T., Xue, Y., Li, Z., Wang, Y., Yang, W., & Xue, C. (2015). Effects of ozone-induced oxidation on the physicochemical properties of myofibrillar proteins recovered from bighead carp (*Hypophthalmichthys nobilis*). *Food and Bioprocess Technology, 8*(1), 181–190.